

Three-Dimensional Photoelastic Stress Analysis of the Dovetail Region of the TF-30 Turbine Engine's Third-Stage Fan

V. J. PARKS and R. J. SANFORD

*Mechanics of Materials Branch
Ocean Technology Division*

December 29, 1978



NAVAL RESEARCH LABORATORY
Washington, D.C.

Approved for public release; distribution unlimited.

SECURITY CLASSIFICATION OF THIS PAGE (When Data Entered)

| REPORT DOCUMENTATION PAGE | | READ INSTRUCTIONS BEFORE COMPLETING FORM |
|---|---|---|
| 1. REPORT NUMBER NRL Report 8276 | 2. GOVT ACCESSION NO. | 3. RECIPIENT'S CATALOG NUMBER |
| 4. TITLE (and Subtitle) THREE-DIMENSIONAL PHOTOELASTIC STRESS ANALYSIS OF THE DOVETAIL REGION OF THE TF-30 TURBINE ENGINE'S THIRD-STAGE FAN | 5. TYPE OF REPORT & PERIOD COVERED Final report on one phase of a continuing NRL problem. | |
| | 6. PERFORMING ORG. REPORT NUMBER | |
| 7. AUTHOR(s) V. J. Parks and R. J. Sanford | 8. CONTRACT OR GRANT NUMBER(s) | |
| 9. PERFORMING ORGANIZATION NAME AND ADDRESS Naval Research Laboratory Washington, D.C. 20375 | 10. PROGRAM ELEMENT, PROJECT, TASK AREA & WORK UNIT NUMBERS NRL Problem F01-29 A5365360-0582 | |
| 11. CONTROLLING OFFICE NAME AND ADDRESS | 12. REPORT DATE December 29, 1978 | |
| | 13. NUMBER OF PAGES 31 | |
| 14. MONITORING AGENCY NAME & ADDRESS (if different from Controlling Office) | 15. SECURITY CLASS. (of this report) UNCLASSIFIED | |
| | 15a. DECLASSIFICATION/DOWNGRADING SCHEDULE | |
| 16. DISTRIBUTION STATEMENT (of this Report) Approved for public release; distribution unlimited. | | |
| 17. DISTRIBUTION STATEMENT (of the abstract entered in Block 20, if different from Report) | | |
| 18. SUPPLEMENTARY NOTES | | |
| 19. KEY WORDS (Continue on reverse side if necessary and identify by block number) Failure analysis Photoelasticity Stress analysis Turbine Engine | | |
| 20. ABSTRACT (Continue on reverse side if necessary and identify by block number) Three-dimensional photoelastic analysis of the disk/blade dovetail region of the TF-30 turbine engine's third-stage fan indicates peak stresses in the disk and blade fillets that are an order of magnitude greater than the average stress in the neck of the disk lug. Maximum stress concentrations found in the fillets of the disk lugs for representative loads are: 9.6 for centrifugal load; 12.6 for centrifugal load with 12% circumferential component; and 10.6 for centrifugal load with an 18% antiplane component. (continued) | | |

20. ABSTRACT (Continued)

The addition of circumferential or antiplane bending components to the centrifugal load increased the peak stress and shifted it toward the region of the fillet where fractures have been observed. The analysis gives quantitative indication of the significance of bending in the failure of disk lugs.

CONTENTS

| | |
|---|----|
| INTRODUCTION | 1 |
| GEOMETRY | 1 |
| LOADING | 1 |
| THREE-DIMENSIONAL PHOTOELASTICITY | 7 |
| EXPERIMENTAL PROCEDURES | 7 |
| ANALYSIS | 11 |
| RESULTS | 12 |
| COMPARISON OF THREE-DIMENSIONAL ANALYSIS WITH TWO-DIMENSIONAL ANALYSIS | 23 |
| DISCUSSION OF RESULTS | 25 |
| Centrifugal Load | 25 |
| Circumferential Load | 25 |
| Antiplane Load | 25 |
| Out-of-Plane Load | 26 |
| Superposition of Loads | 26 |
| SCALING | 26 |
| CORRELATION OF STRESS WITH FAILURE ANALYSIS | 27 |
| SUMMARY | 27 |
| REFERENCES | 28 |

THREE-DIMENSIONAL PHOTOELASTIC STRESS ANALYSIS OF THE DOVETAIL REGION OF THE TF-30 TURBINE ENGINE'S THIRD-STAGE FAN

INTRODUCTION

Several in-service failures of the TF-30 turbojet engine used in the F-14 aircraft have been traced to cracking in the blade/disk assembly of the third-stage fan. A series of reports [1-4] has addressed various stress-analysis and fracture-mechanics aspects of the problem and can be consulted for background. Of particular interest to the present study is NRL Report 8149 [1], which presented a two-dimensional stress analysis of the region of failure. This is an extension of that study and reports the three-dimensional photoelastic stress analysis of the same region, for the previously studied load and for additional loading conditions.

GEOMETRY

Figure 1 shows an overall view of the third-stage fan, 36 blades mounted on a central disk. Failures have occurred in the dovetail joints that held the blades in the disk, specifically in the teeth of the disk lugs in the dovetail joint. Figure 2 shows two typical failure surfaces on a disk removed from service.

As in the two-dimensional study, it was decided to model two blades of the fan and the accompanying disk segment. The model of the disk segment consisted of three lugs. Since the failures were primarily in one fillet of the disk lug, it was decided that the center lug of the three would be adequate to represent the actual stressed condition of the lug. The disk model and the disk segment from which it was replicated are shown in Fig. 3. An engine blade and its model are shown in Fig. 4. The blade was modeled, up to the upper shroud. The blade models were reinforced as shown to insure that failure of the model did not occur in gripping the blades.

LOADING

The largest load on the disk and blades is clearly the centrifugal load on the blade. However, the location of the failure suggests that additional loads combine with the centrifugal load to cause failure. To represent a number of possible loadings, both steady state and vibrating, it was decided to analyze for the stresses due to three blade loads:

1. The centrifugal load only
2. The centrifugal load combined with a bending load in the plane of the disk (to simulate the in-plane vibration)

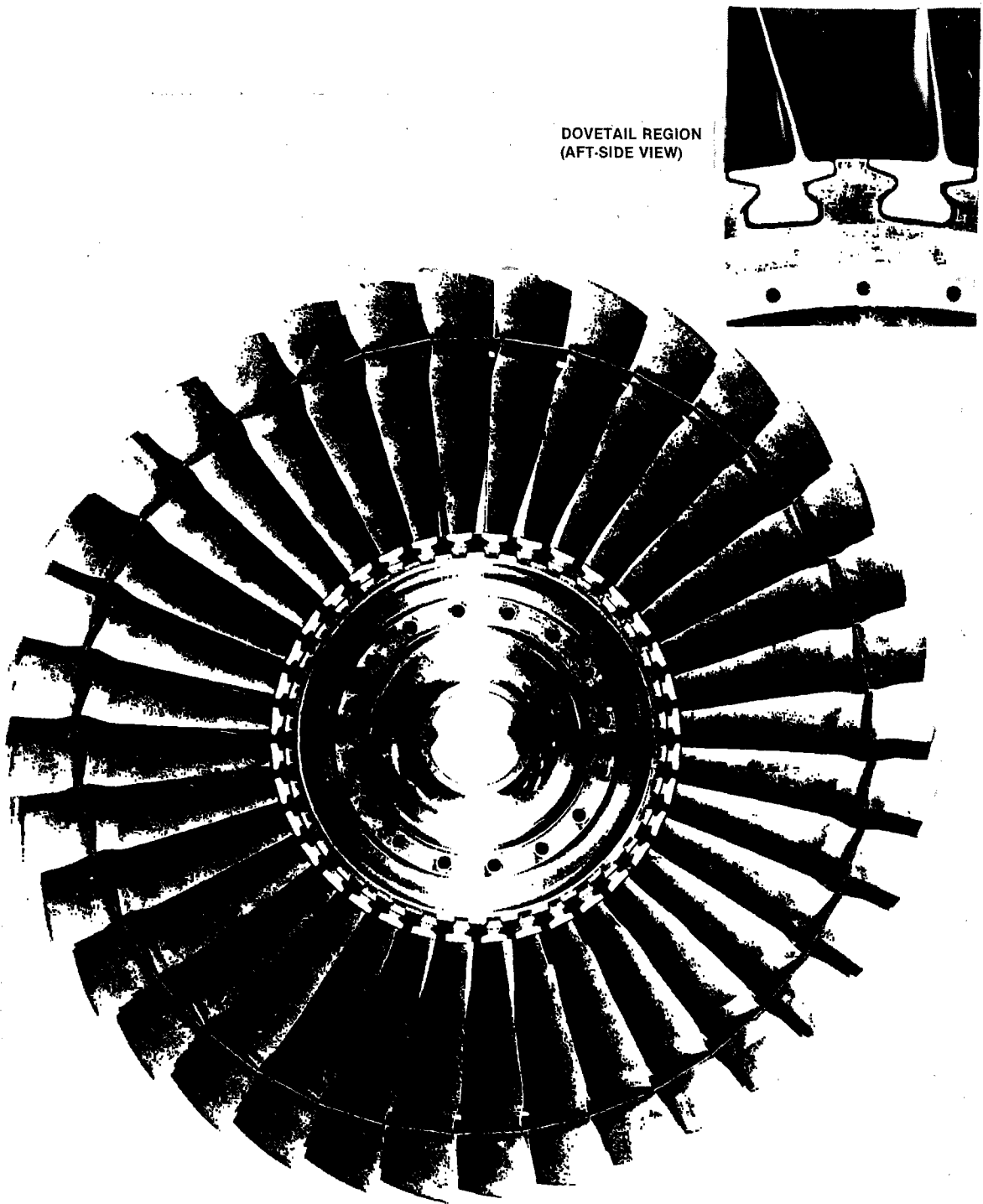


Fig. 1 — Disk and 36 blades in third stage of engine (fore-side view). Dovetail region (aft view)

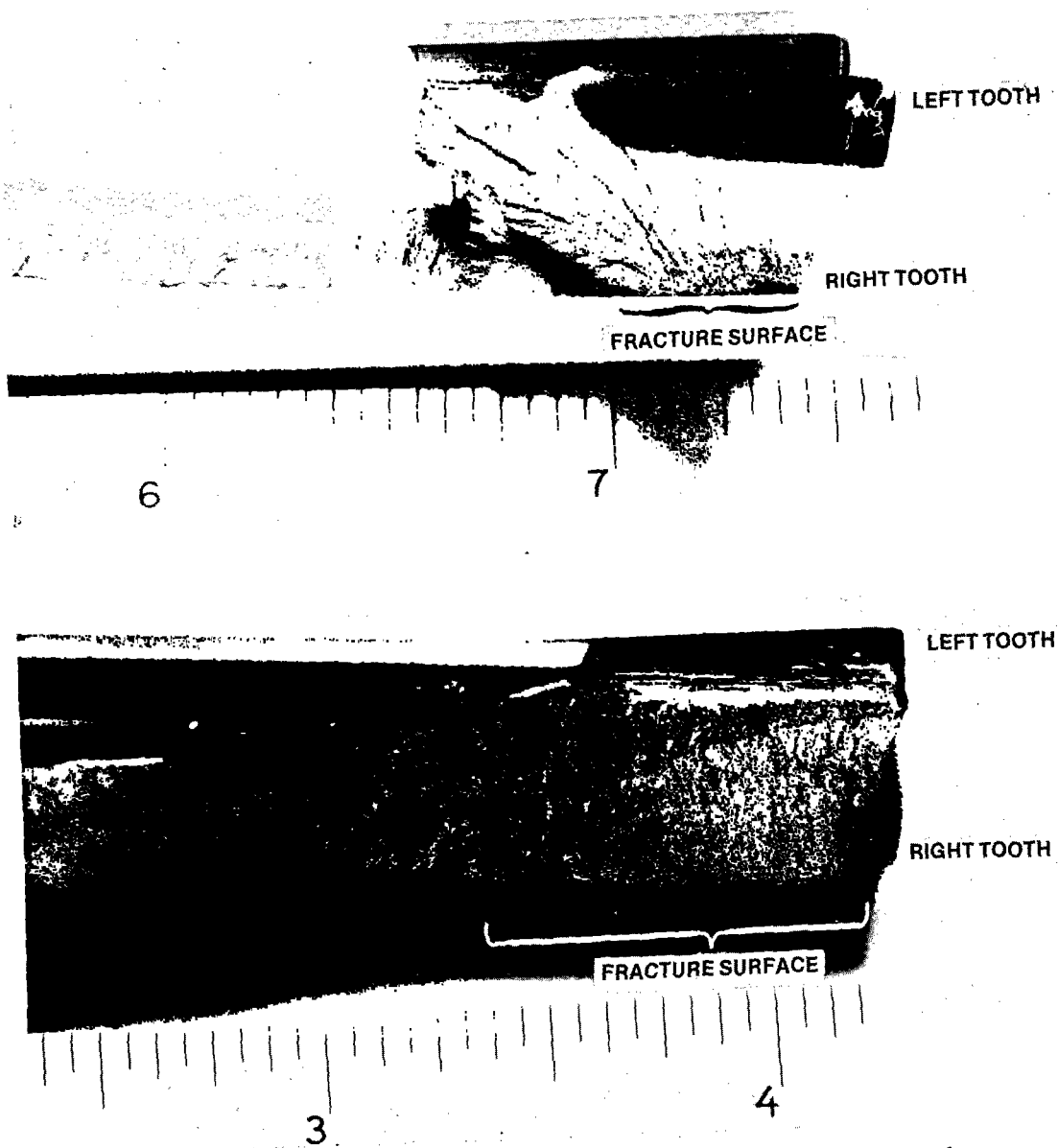


Fig. 2 — Two cracked lugs broken from disk show fracture surfaces of cracks

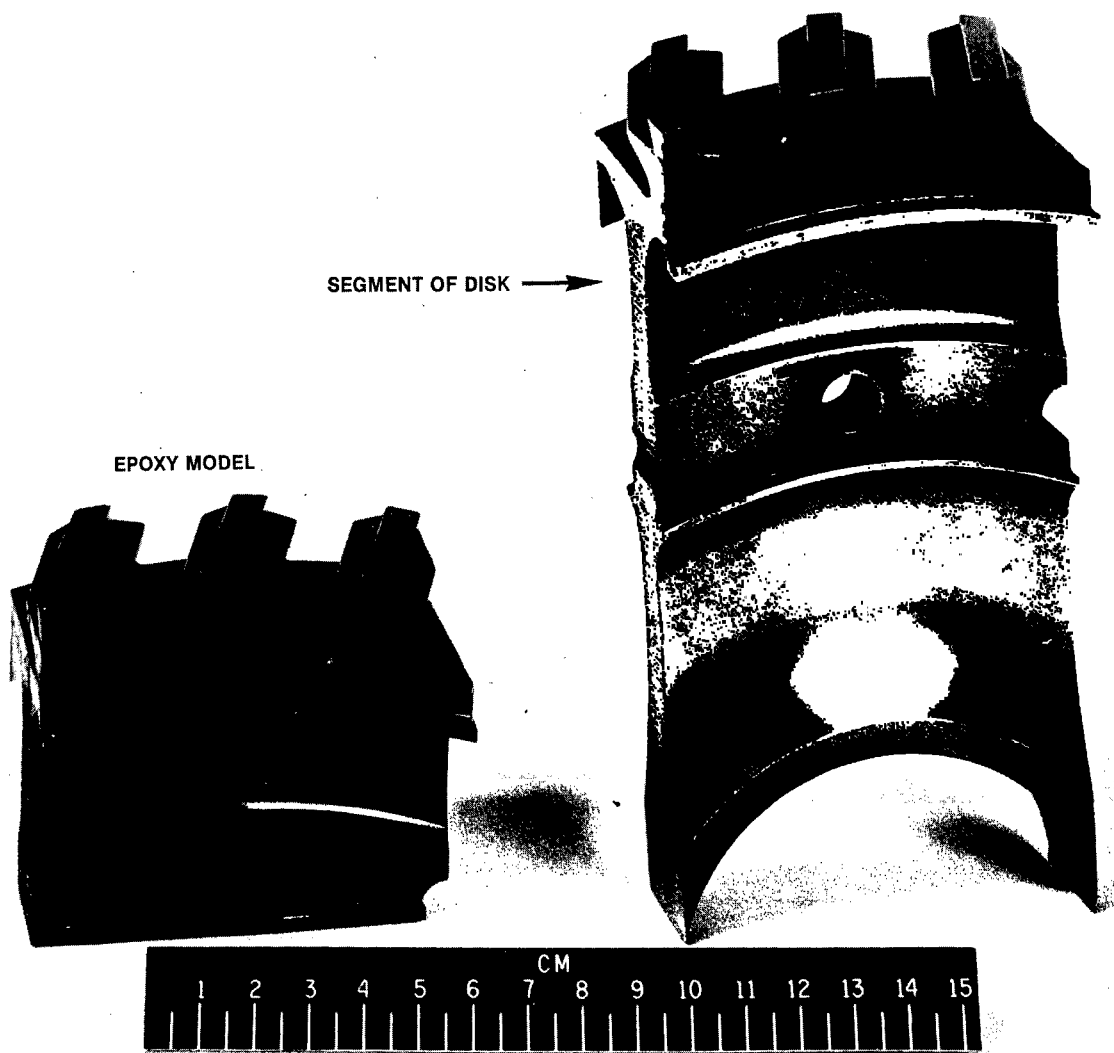


Fig. 3 — Epoxy model of disk alongside disk segment from which it was replicated

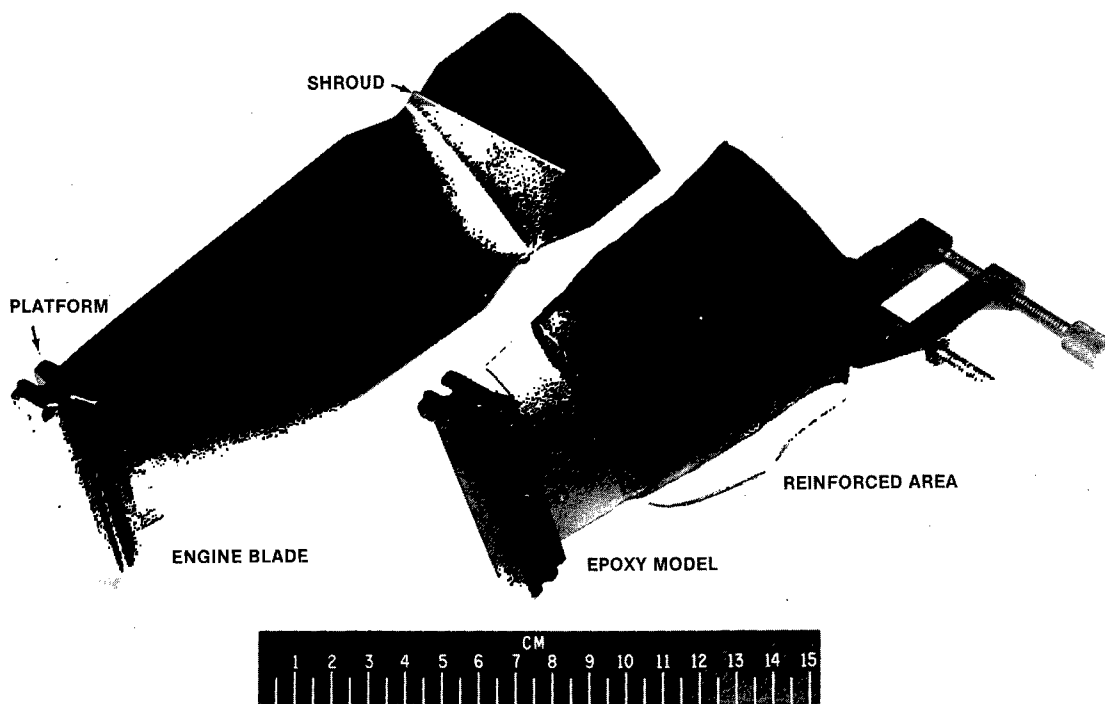


Fig. 4 — Engine blade and replicated epoxy model

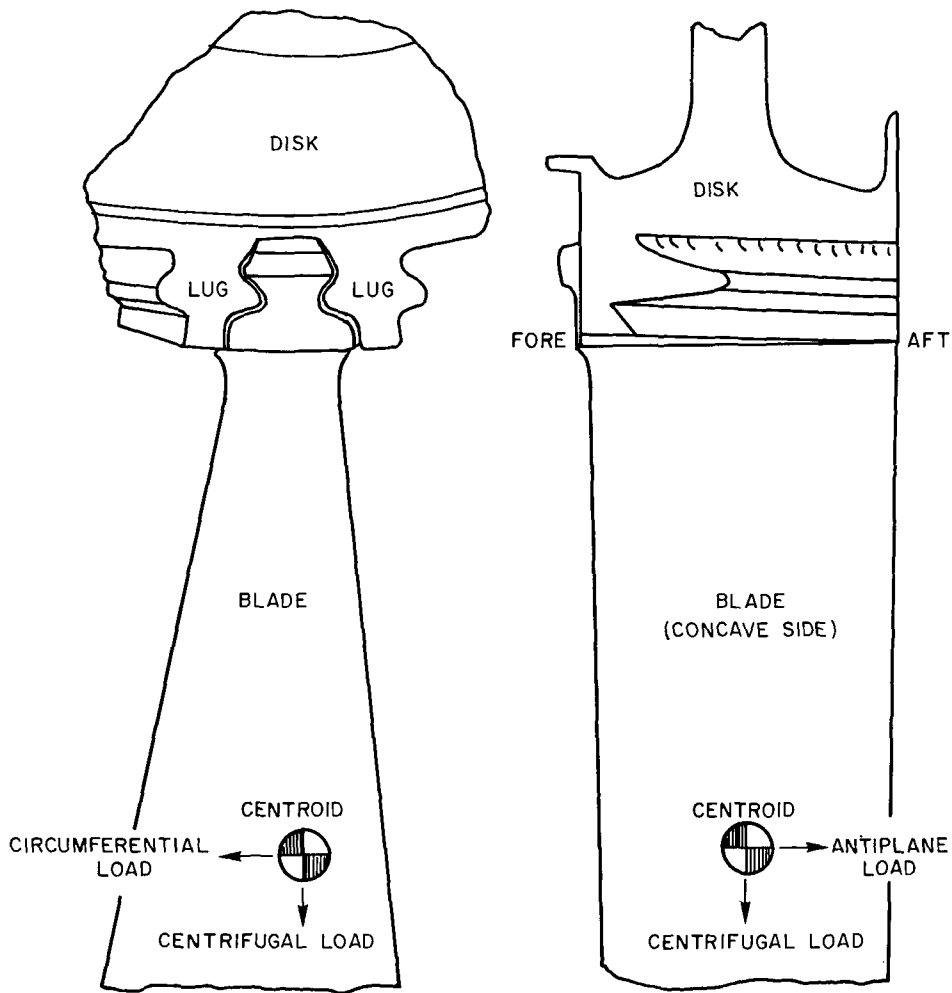
3. The centrifugal load combined with a bending load perpendicular to the plane of the disk (to simulate antiplane vibrations).

Figure 5 shows the loads applied to the models. The centrifugal loads were simulated by a radial force applied at the centroid of each blade. The in-plane bending loads were simulated by forces acting at the blade centroids in the circumferential direction, clockwise when viewed from the front of the engine. The antiplane bending loads were simulated by forces acting at the blade centroids in the fore-to-aft direction. The combined centrifugal and bending loads were produced by forces acting through the blade centroids. These forces had both radial and circumferential, or antiplane, components.

If the blades and disk were a single part it would have been possible (and convenient) to apply the centrifugal and bending loads separately and combine them in any desired proportions, using the principle of superposition. However, because the forces are transmitted through the bearing surfaces between the disk and the blades, and permit only net compressive forces, combined centrifugal and bending loads were chosen that would apply compressive loads over the whole bearing surface (i.e., liftoff was not permitted).

The results from both combined loadings were modified by subtracting the results from the centrifugal load, which yielded the stresses due to bending alone. Stresses are presented for each of the actual loadings and for the three individual loads: (a) centrifugal, (b) bending in the plane of the disk, (c) antiplane bending of the disk.

PARKS AND SANFORD



| LOADING | LOAD COMPONENTS ON EACH BLADE MODEL | | |
|-------------------------------|-------------------------------------|-----------------|-----------|
| | CENTRIFUGAL | CIRCUMFERENTIAL | ANTIPLANE |
| CENTRIFUGAL | 14.7 lb | 0 | 0 |
| CENTRIFUGAL - CIRCUMFERENTIAL | 6.91 lb | 0.82 lb | 0 |
| CENTRIFUGAL - ANTIPLANE | 7.14 lb | 0 | 1.26 lb |

Fig. 5 - Loads applied to blade and disk models

The two bending loads were recombined with the centrifugal load in various proportions to describe a number of possible states of stress, depending on the ratio of bending to centrifugal load.

Finally, the analyses of the two bending components were combined vectorially with each other to obtain the stress distribution for a bending-load component acting at given angles about the stacking axis of the blade.

THREE-DIMENSIONAL PHOTOELASTICITY

Three-dimensional photoelasticity is a method in which a model of the structure is manufactured from a suitable plastic (currently epoxy) and subjected to loads corresponding to the loads in the structure. The loads are the same in direction and in proportion to those loads on the structure, but of a much smaller magnitude. In many cases, including the one studied here, it is sufficient to model and load only a portion of the structure.

The loaded model of the structure is heated to a temperature at which the plastic softens and becomes "rubbery." In that state, small loads are sufficient to subject the model to measurable strain and deformation. While still under load the model is slowly cooled. This "freezes in" the deformations and the photoelastic effect associated with the strains. In this state the model can be cut apart and the photoelastic effect on any plane of the model analyzed. Within the linear range of the material, certain fringes of the photoelastic effect (called isochromatics) are proportional to both stress and strain, thus allowing a stress analysis throughout the three-dimensional body. The isochromatic fringes give the tangential stresses on all free surfaces of the structure, and the maximum shear stresses at all points in the interior of the structure. Since failure occurs on the surface of the structure, the stresses reported here are all tangential surface stresses.

EXPERIMENTAL PROCEDURES

The common method used in manufacturing three-dimensional photoelastic models is to machine the models from blocks of epoxy. Because of the complexity of the blades and disk studied here, the models were cast directly in molds. Casting epoxy normally creates an undesirable skin effect called *rind*. Various epoxy formulations were tested to find one with a minimum amount of rind. The epoxy formulation and curing procedures finally chosen were ones developed by Cernosek [5].

Figure 6 shows the disk mold and the disk model. The molds were made from silicone rubber cast directly over the engine parts and cut along suitable parting lines for removal. Each mold has an outer jacket of silicone rubber to hold the mold parts and prevent leakage [6]. The incorporation of this outer jacket into the molding procedure proved to be a significant advance in simplifying the casting and improving the accuracy of replication. Each mold was used to make a number of models.

Each batch of epoxy that was cast contained a complete set of model components; a disk segment, two blades, and sufficient calibration specimens to completely characterize the batch of material.

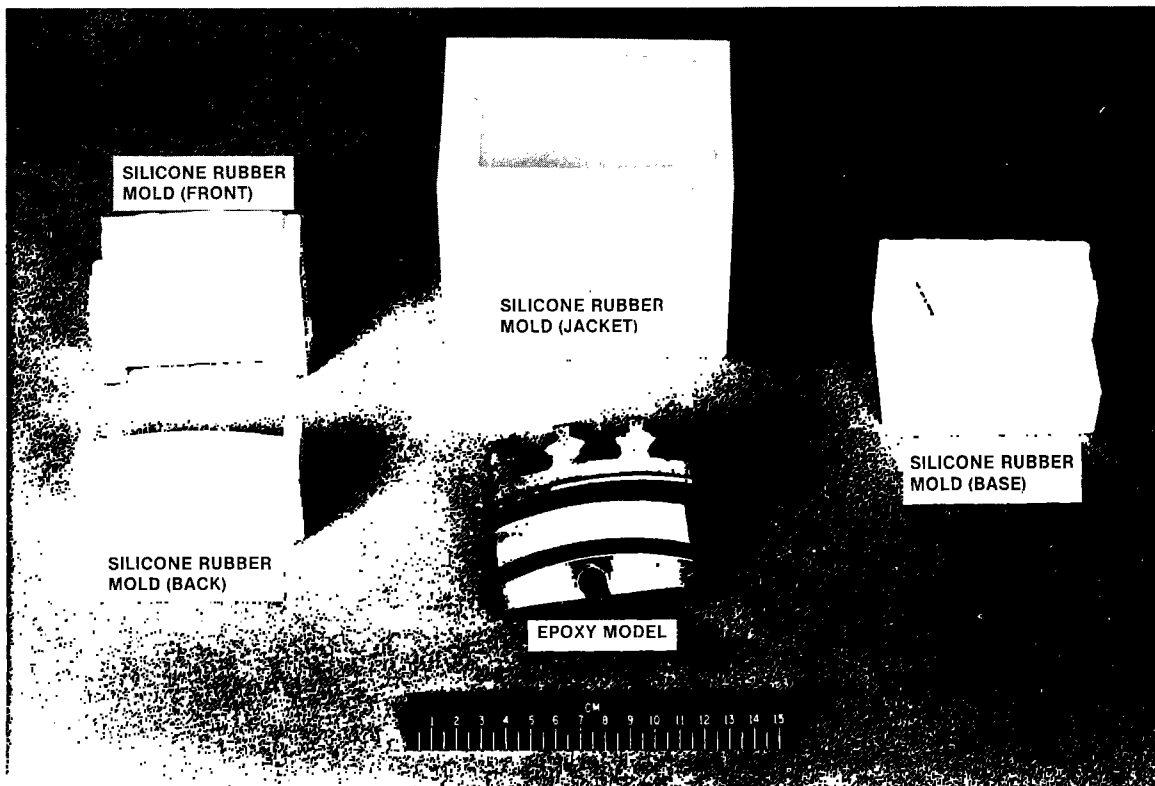


Fig. 6 — Epoxy model disk surrounded by silicone rubber mold parts

Each set of models was loaded with one of the loads shown in Fig. 5. The loaded models were placed in an oven along with a circular epoxy calibration specimen loaded in diametral compression. The oven was heated slowly until the epoxy reached its critical temperature; it was then cooled slowly, following the recommended procedures [5]. The cooling locked in the deformation and photoelastic pattern.

The models were sliced in various ways to study the stress distribution. However, the primary analysis was conducted on slices cut from both disk and blades, parallel to the plane of the disk. Figure 7 shows a series of slices of the disk model and an uncut disk model. All these slices were rotated 15.5° so as to be viewed and photographed perpendicular to the cross section of the disk slot and the cross section of the dovetail of the blade that fits in the slot. And the stresses obtained in analysis are stresses in these cross-sectional planes. The slices were immersed in a fluid of the same index of refraction as the epoxy so as to avoid polishing the slices and also to eliminate unwanted refraction of light.

Figures 8 and 9 are isochromatic patterns of slices from a disk lug and blade, respectively, after a simulated centrifugal load was frozen in. The stresses reported here are the stresses in the plane of the cross section. However in Figs. 8 and 9 the fringes at different circumferential positions will represent slightly different cross sections of the blade and disk lug.

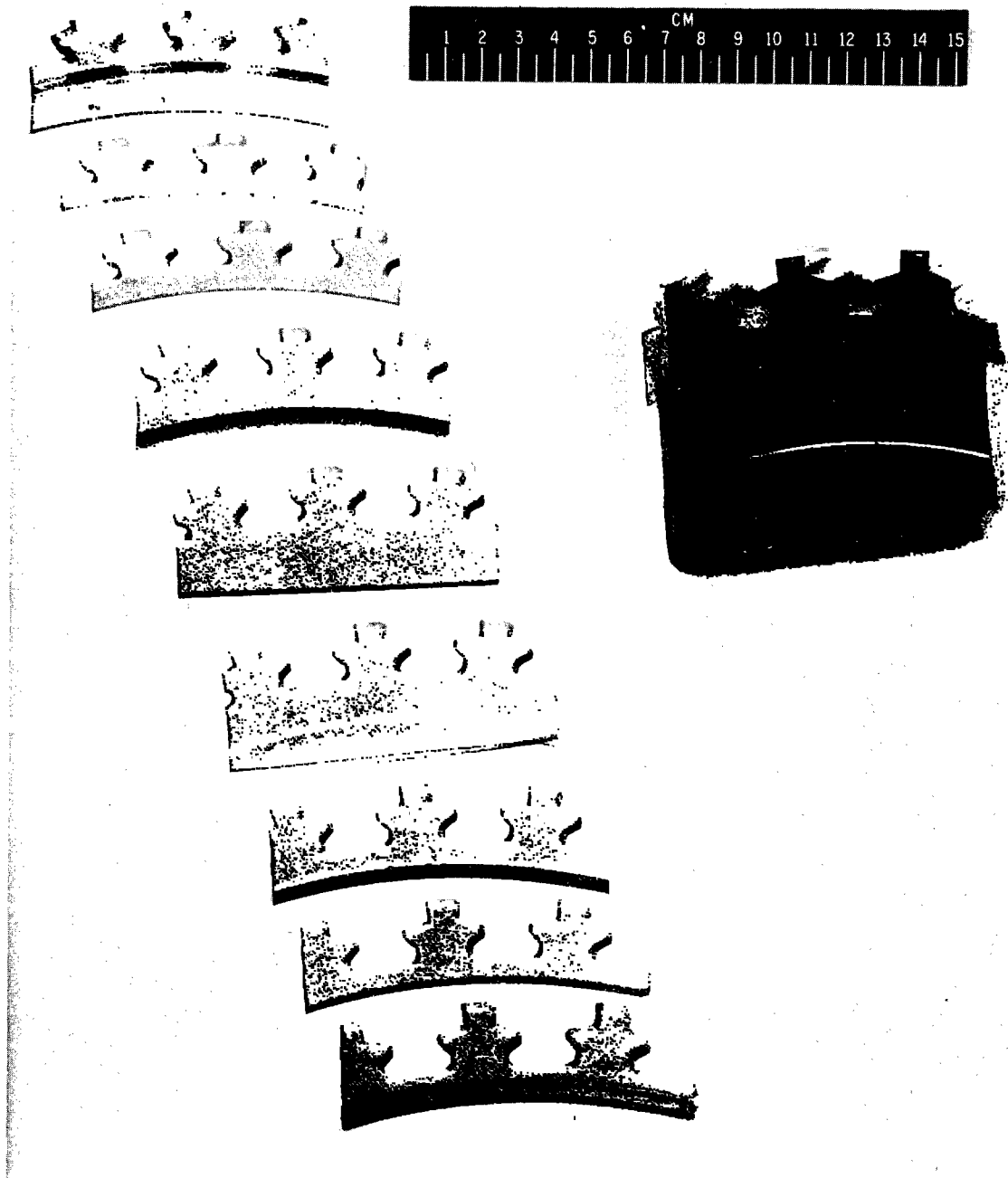


Fig. 7 — Epoxy model and a set of slices of the disk

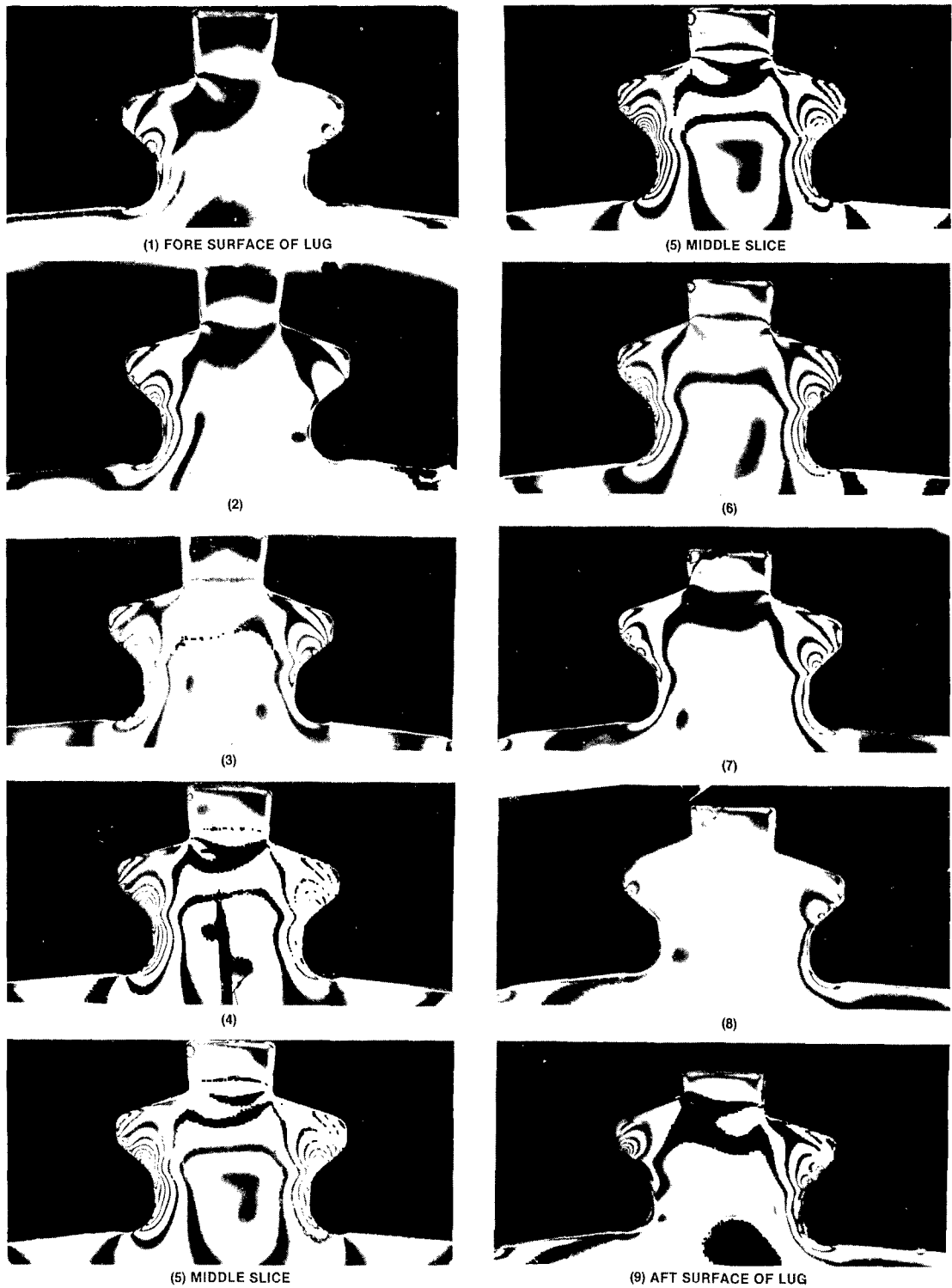


Fig. 8 — Isochromatic patterns of a series of disk slices. Note variations from end to end.

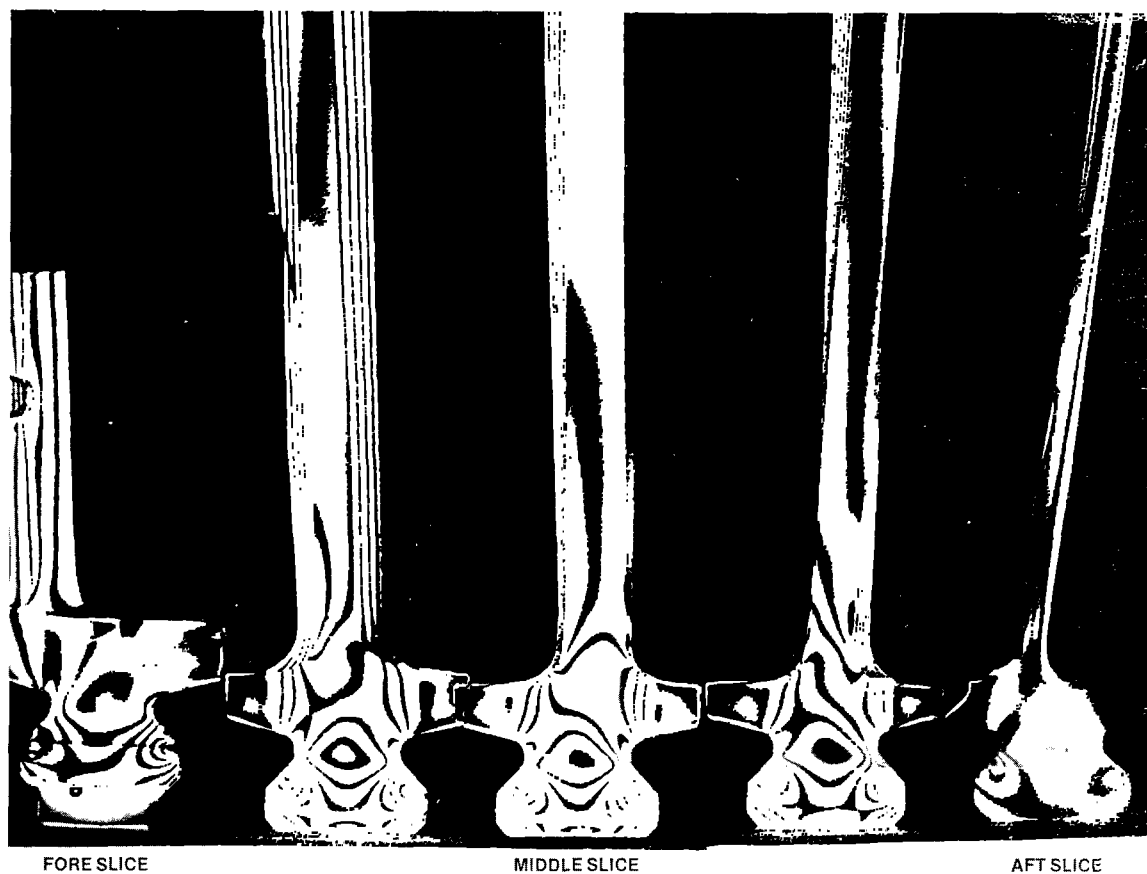


Fig. 9 — Isochromatic patterns of a series of blade slices

ANALYSIS

The thickness of all the slices was measured and then adjusted to account for the 15.5° viewing angle. Fringes in each pattern were ordered (as will be illustrated later in the results), and the maximum fringe orders in the fillets were estimated to a tenth of a fringe. In cases where the fringes were very dense, the slice was thinned to reduce the number of fringes.

The relation of the isochromatic fringes to the stresses on the free boundaries of the models is

$$\sigma_t = \frac{nf}{t},$$

where

σ_t is the tangential stress on the model boundary in the plane in which the fringe is viewed

n is the fringe order at the point of stress

t is the optical thickness of the material, at the point, in the viewing direction,

f is the material fringe value (the photoelastic constant).

Material fringe values were obtained for each test, using the known theoretical solution for the stresses at the center of the calibration specimen in diametral compression. The f -values varied from 2.05 to 2.26 psi-in./fringe.

All stresses were normalized in terms of a known stress. That is, the results are given as stress ratios (stress-concentration factors); the ratio of the analyzed stress to the known stress. The average stress across the neck of the disk lug was chosen as the most convenient known stress. Thus modified, the stresses represent the stresses in the engine.

In the engine, if the load is known, the average stress can be obtained by dividing the centrifugal component of the load by the area of the neck (1.14 sq. in.). In the model loading, the total load was measured in each test, and for the bending tests the angle of the load from the radial direction was also measured. In the bending tests the centrifugal component of the load was used to obtain the average stress.

The average stress in the models was obtained by dividing the centrifugal load or centrifugal component of load by the area of the neck. This stress was in turn divided into the stresses obtained from Eq. (1) to determine the stress-concentration factors in the fillets. Note that this average stress is used even in the blade analysis to allow direct comparison of disk and blade fillet stresses. If the stress-concentration factor in the blade is desired in terms of the average stress in the neck of the *blade*, the reported stress-concentration factor must be multiplied by 0.78, the ratio of the areas of the blade neck and the disk neck.

RESULTS

Figures 10 and 11 show the distribution of maximum tensile stresses along the length of the teeth in the fillets of the disk (Fig. 10) and blade (Fig. 11) when subjected to centrifugal load.

Figures 12 and 13 are the stress distributions in the disk for in-plane and antiplane bending in combination with centrifugal load as tested. The in-plane bending force was 12% of the centrifugal force; the antiplane bending force was 18% of the centrifugal force.

Figures 14 and 15 are the components of the fillet stresses due to 10% bending alone.

Figures 16, 17, and 18 show the bending stresses (Figs. 14 and 15) recombined with the stresses due to centrifugal load (Fig. 10) in various proportions, for the right tooth, to indicate how the stress distribution is modified by bending. These curves were developed by adding to and subtracting from the stresses in Fig. 10, multiples of the stresses in Figs. 14 and 15.

Figures 17 and 18 both show the antiplane bending load combined with the centrifugal load. They differ only in that in Fig. 17 the anti-plane stresses are *added* to the centrifugal

stresses, where as in Fig. 18 they are subtracted. Figure 18 illustrates the stress distribution obtained with an antiplane load in the opposite direction to the one actually applied. Since such combinations show maximum stresses away from the failure region, they are considered less significant and only one such curve is shown.

Figure 19 combines the bending stresses given in Figs. 14 and 15 for the right tooth, in vectorial proportions to represent the stresses due to a bending load of 10% of the centrifugal load acting at an angle θ from the plane of the disk about the stacking axis of the blade. (θ is sketched in the figure.)

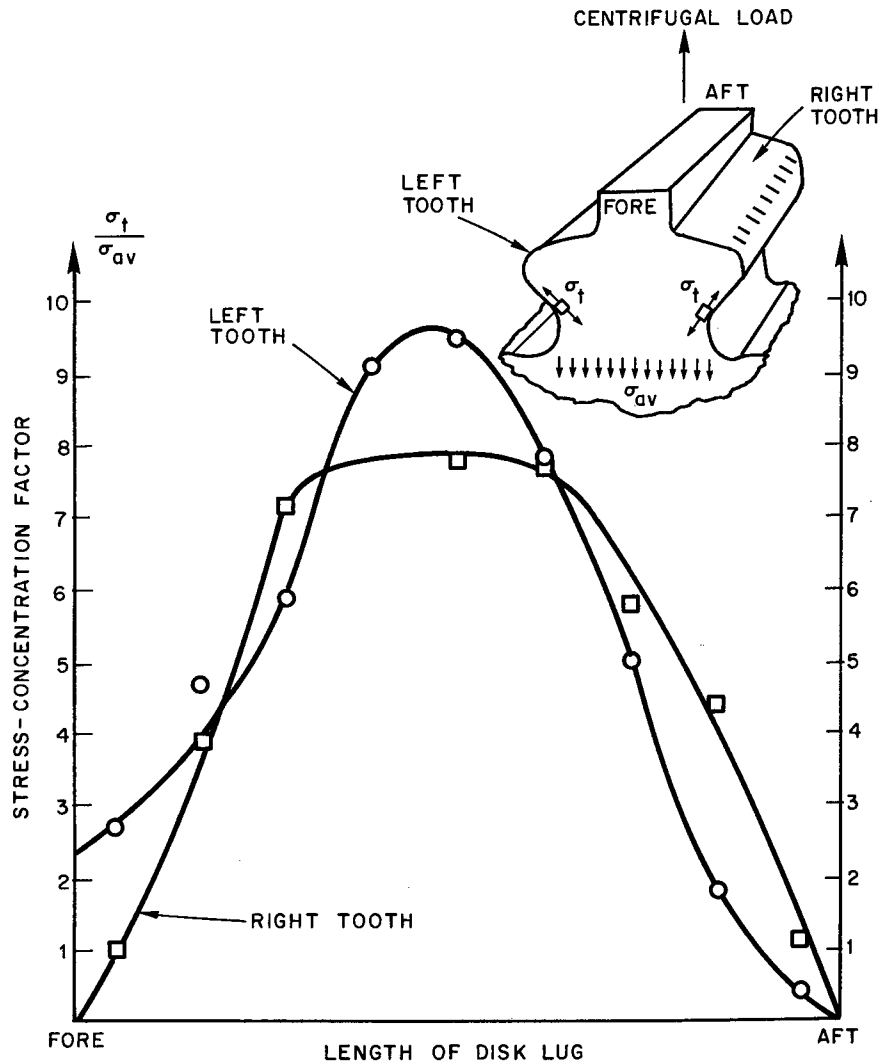


Fig. 10 — Stress-concentration factors in fillets of disk lug teeth under a radial load, simulating the centrifugal load

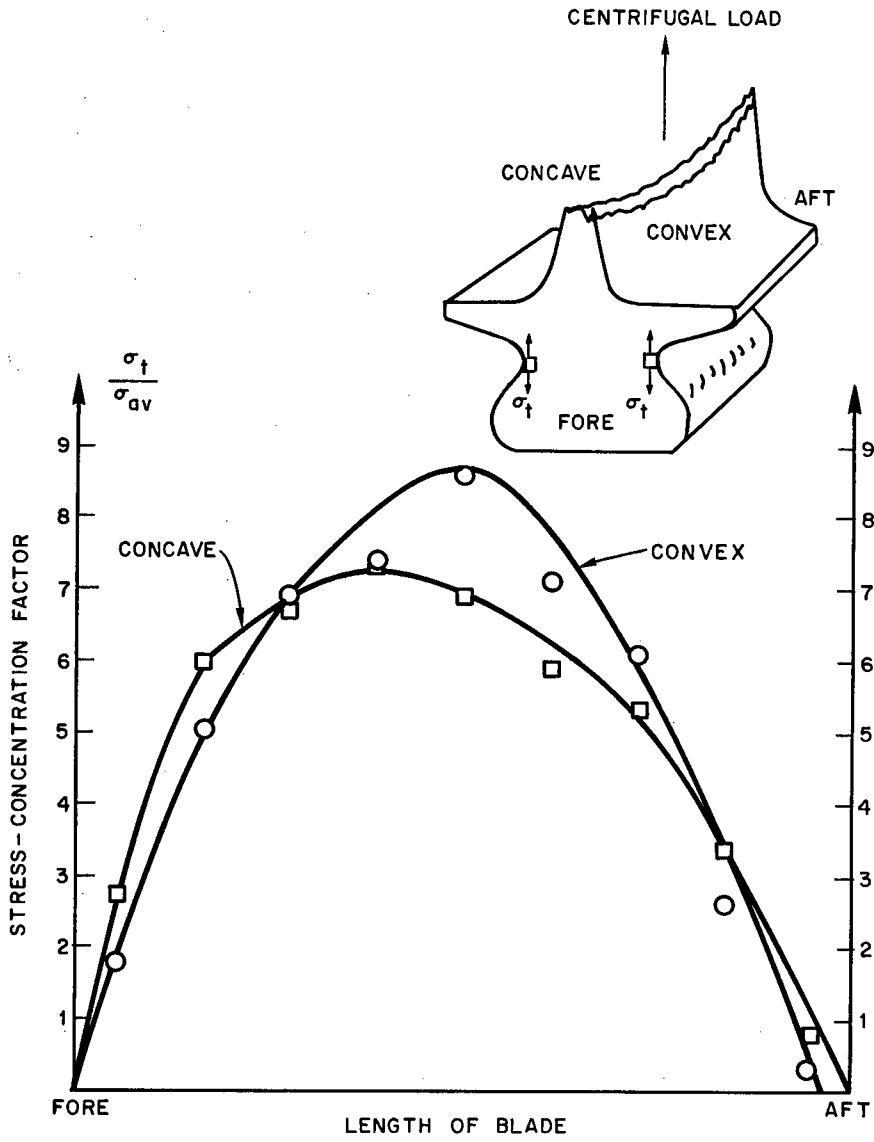


Fig. 11 — Stress-concentration factors in fillets of blade teeth under radial load, simulating the centrifugal load

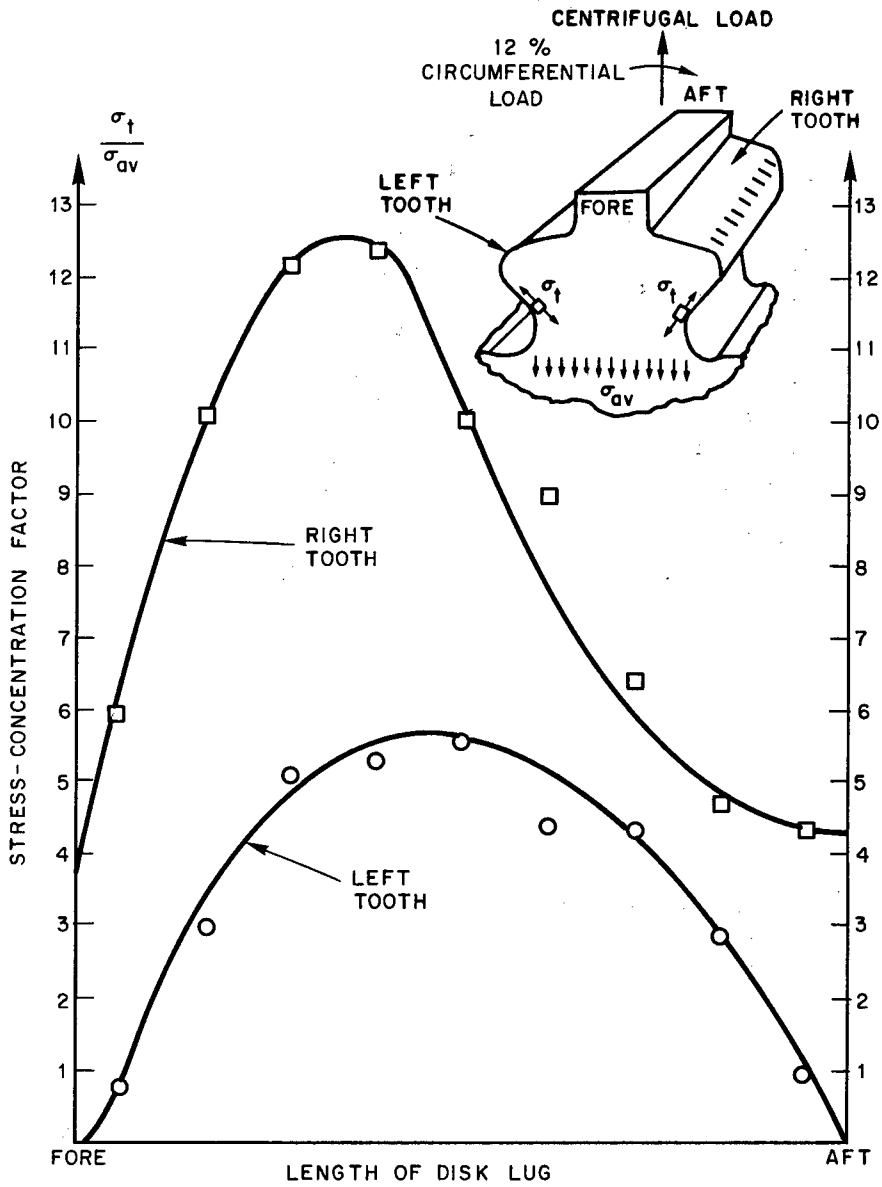


Fig. 12 — Stress-concentration factors in fillets of disk lug teeth under a combined centrifugal and clockwise circumferential load (12% of centrifugal load)

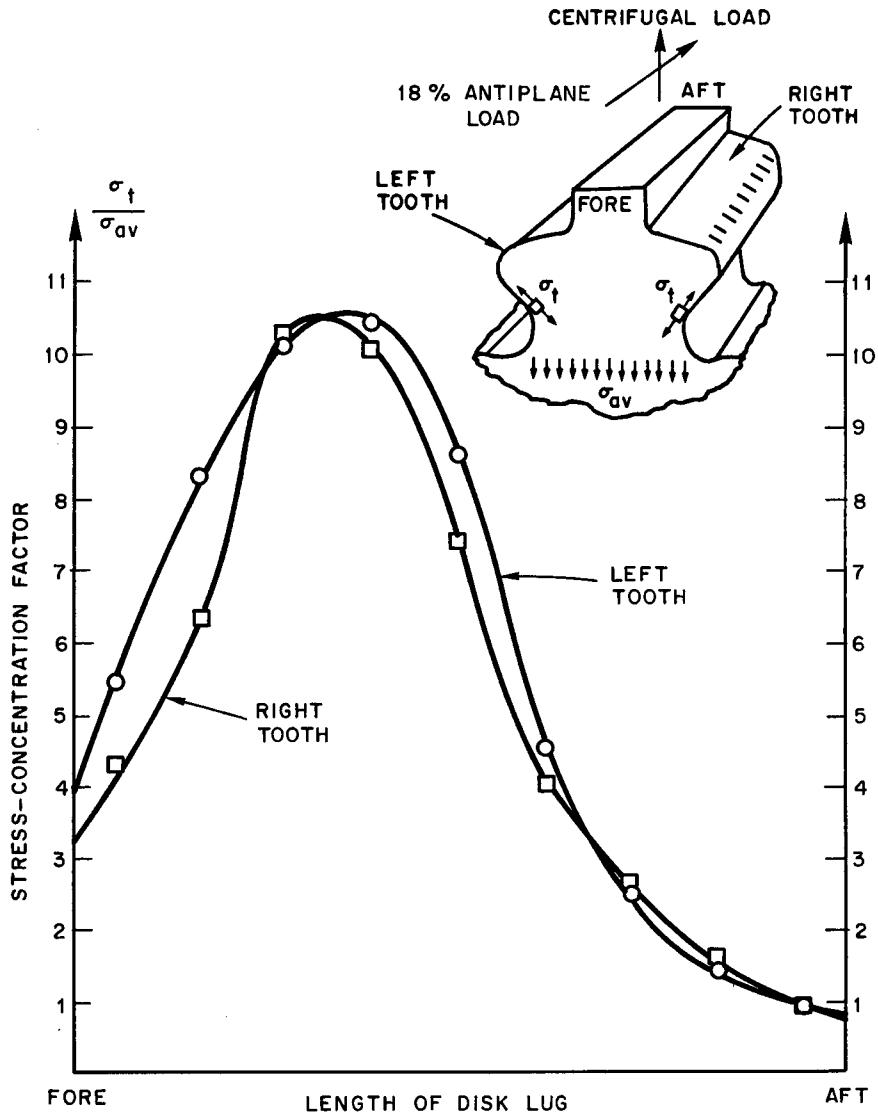


Fig. 13 — Stress-concentration factors in fillets of disk lug teeth under a combined centrifugal and antiplane load (18% of centrifugal load)

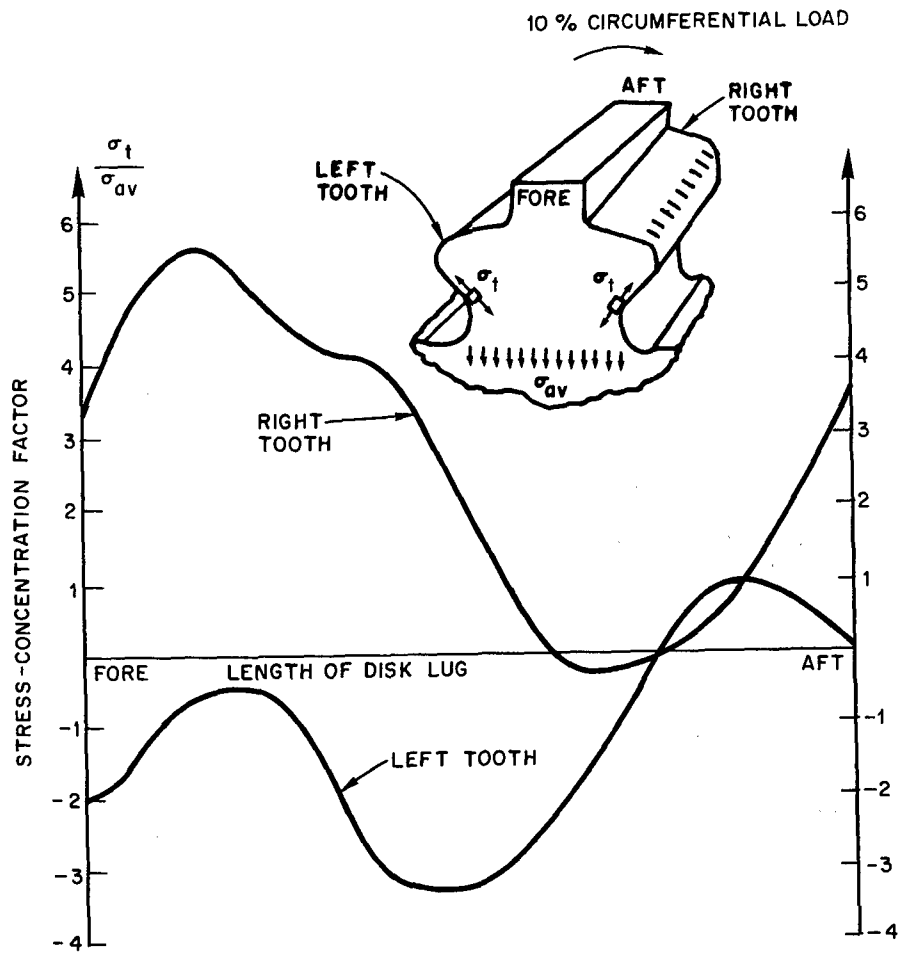


Fig. 14 — Stress-concentration factors in fillets of disk lug teeth due to a clockwise circumferential load of 10% of the centrifugal load

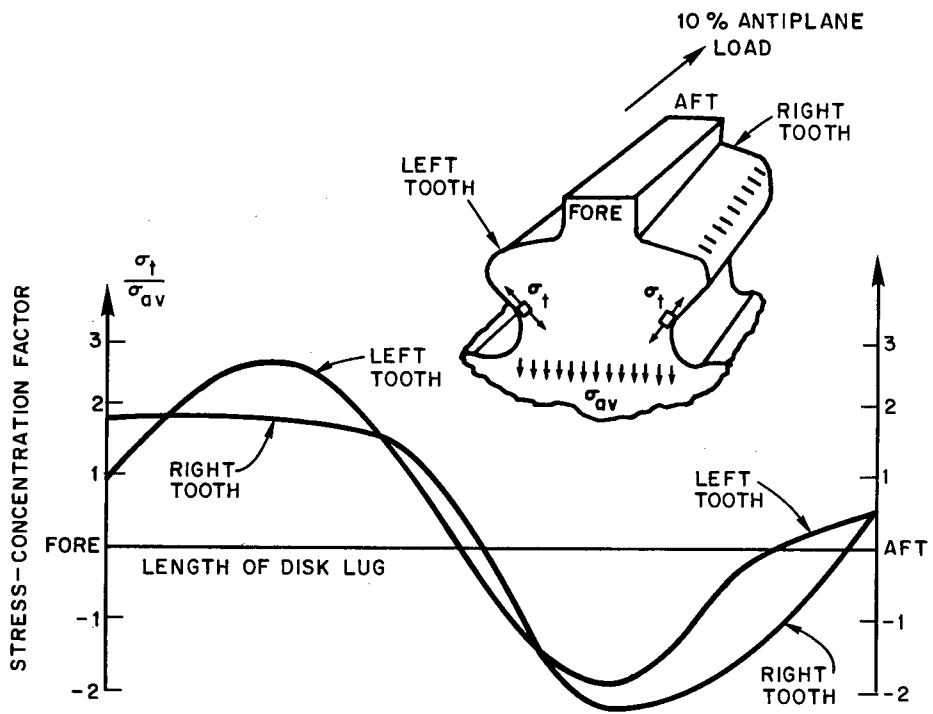


Fig. 15 — Stress-concentration factors in fillets of disk lug teeth due to an antiplane load of 10% of the centrifugal load acting from fore to aft

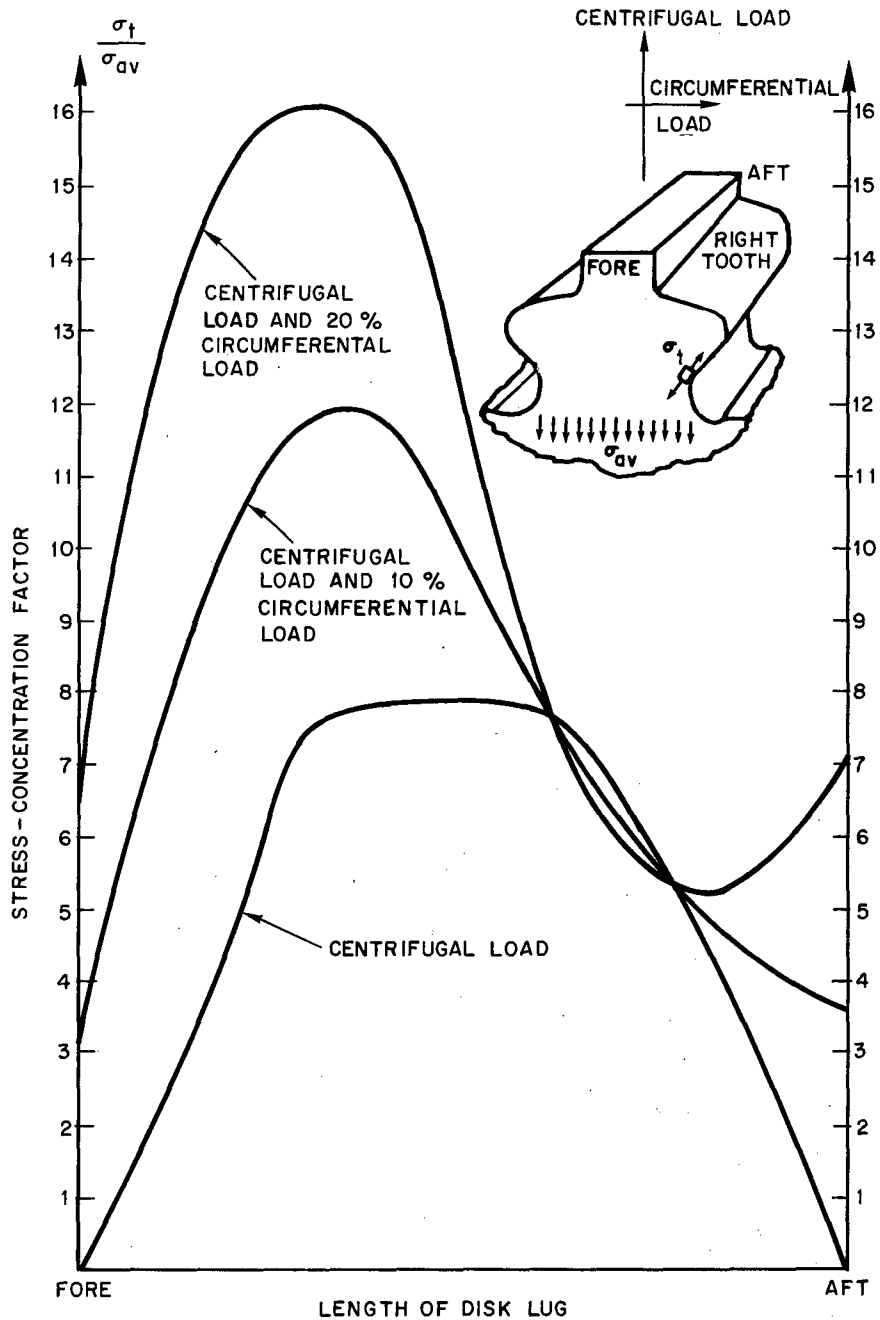


Fig. 16 — Stress-concentration factors in the fillet of the right tooth of the disk lug under centrifugal load and various amounts of circumferential load

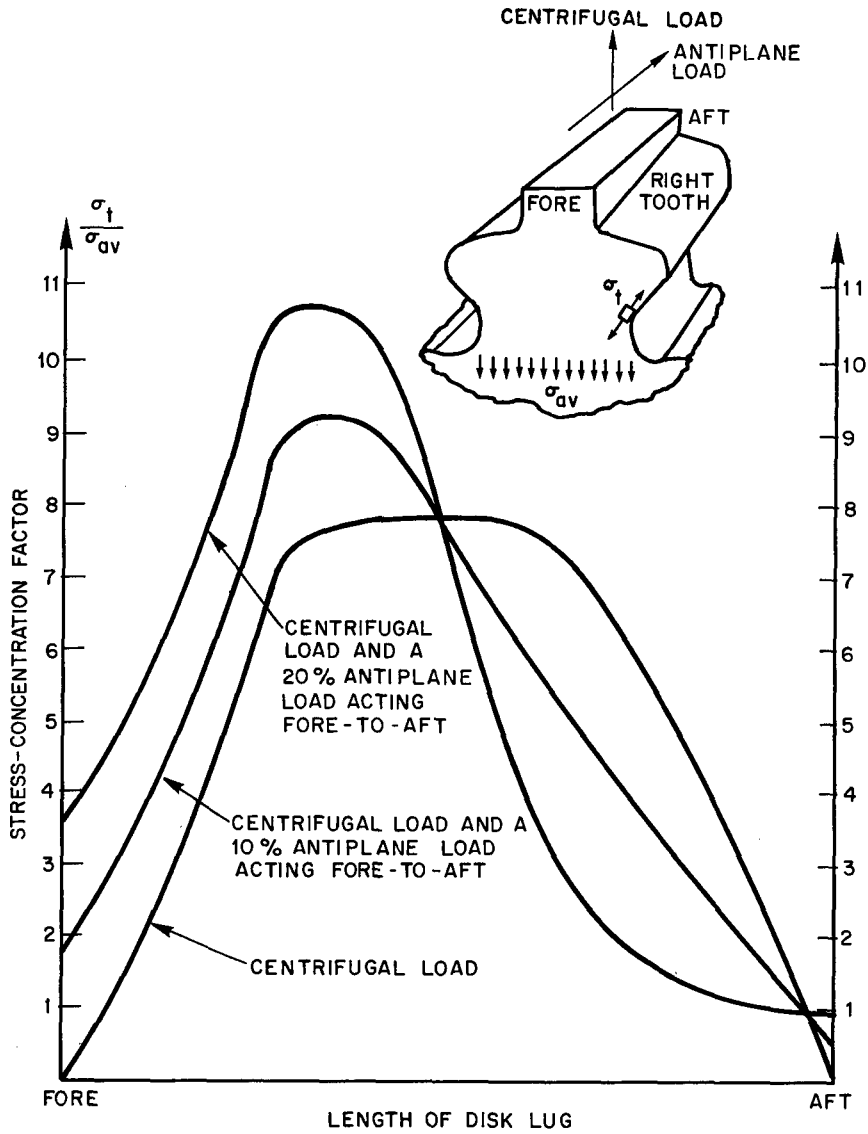


Fig. 17 — Stress-concentration factors in the fillet of the right tooth of the disk lug under centrifugal load and various amounts of antiplane load acting fore to aft

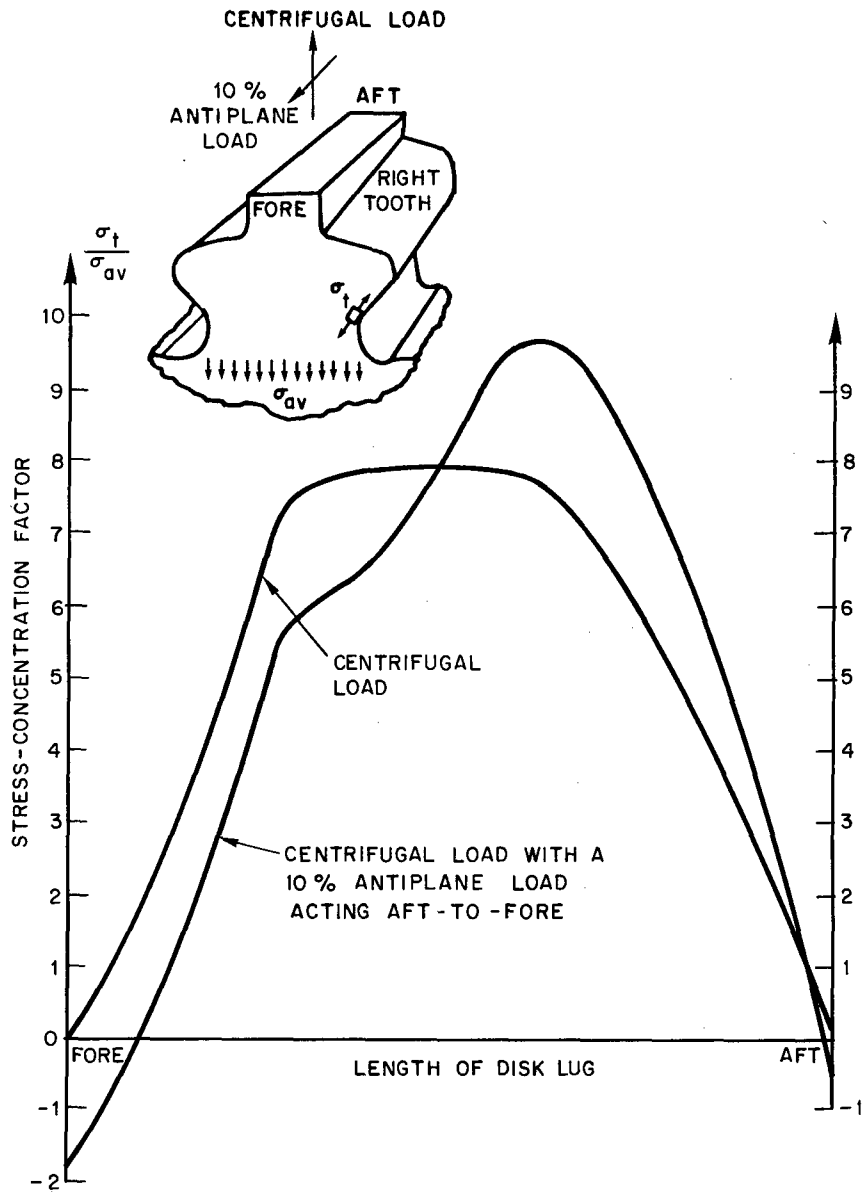


Fig. 18 — Stress-concentration factors in the fillet of the right tooth of the disk lug under centrifugal load and an antiplane load of 10% of the centrifugal load acting aft to fore

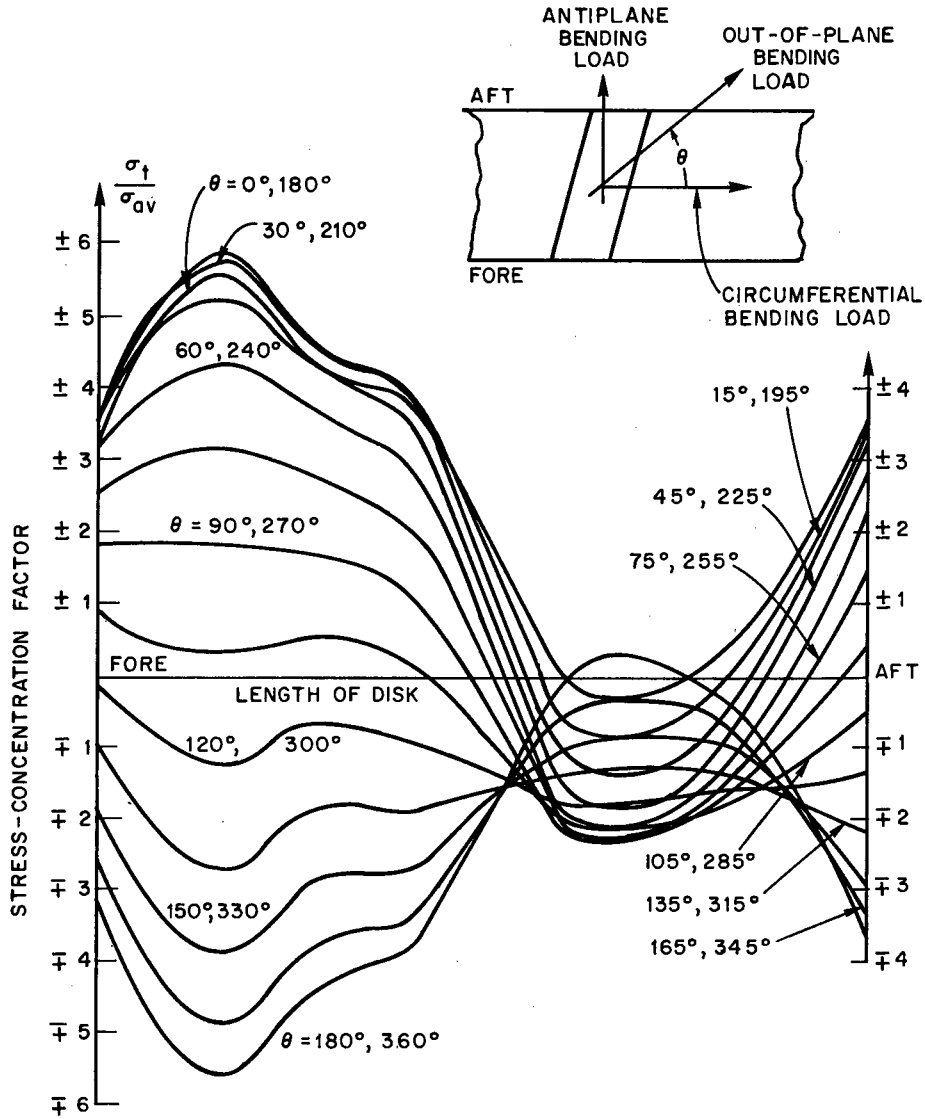


Fig. 19 — Stress-concentration factors in the fillet of the right tooth under bending components of load that are 10% of the centrifugal load, shown for every 15° position around the blade

COMPARISON OF THREE-DIMENSIONAL ANALYSIS WITH TWO-DIMENSIONAL ANALYSIS

Figure 20 shows the comparison of the photoelastic pattern obtained from the two-dimensional analysis with a pattern in a selected slice taken from the three-dimensional model of the disk lug subjected to radial load. The magnitude of the fringes is about the same. This was arranged by choice of loads and thicknesses, to emphasize the similarity of the distribution (the proportions) of fringes over the cross section. Clearly, the two-dimensional model gives a valid analysis of the stress *distribution* over the cross section of the

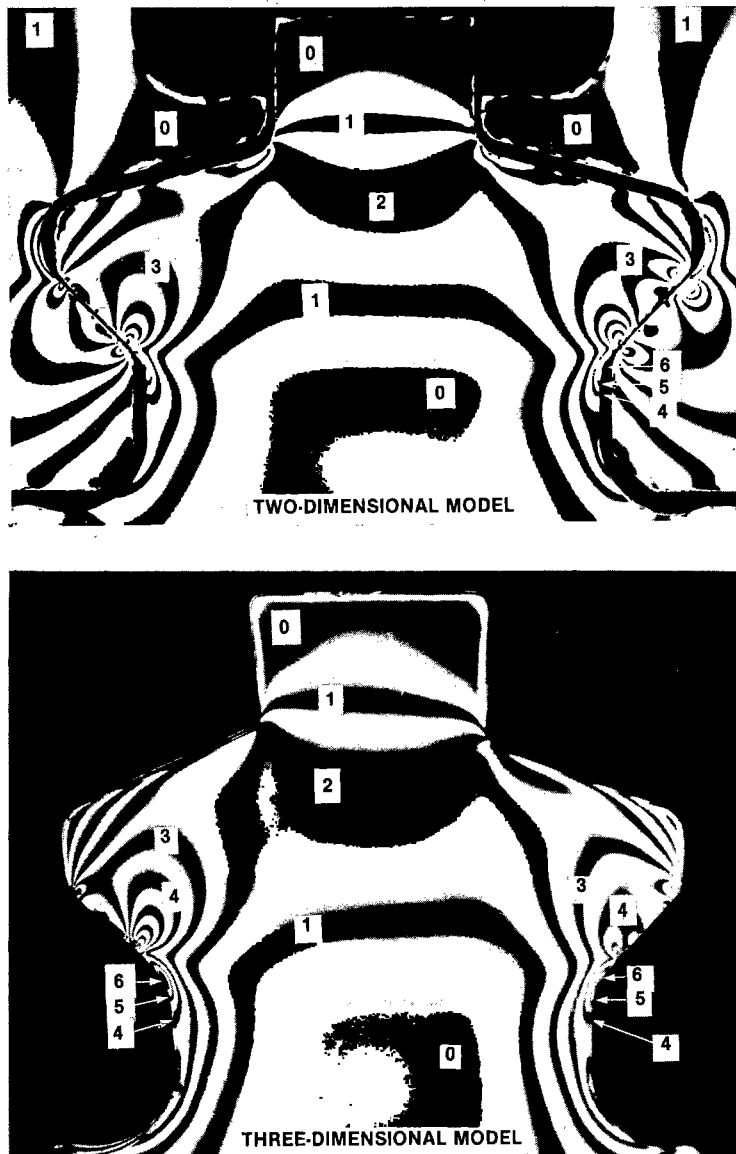


Fig. 20 — Comparison of two- and three-dimensional isochromatic patterns of disk lug

model. However, analysis of all the slices in the three-dimensional model indicates a marked variation in the stress-concentration factors in the direction *perpendicular* to the cross section (see Fig. 9). Comparison of the results from the 2-D and 3-D analysis indicates that the stress-concentration factors for the 3-D case in the central region of the disk lug and blade are about twice what was found in the two-dimensional study. The two-dimensional study gives a good approximation of the average over the length of the teeth. The doubling of stress in the central region is balanced by sharp dropoffs of the stresses at both fore and aft ends of the teeth. Table 1 shows how the stress-concentration factors obtained in the two-dimensional study [1] compare with the maxima and averages obtained in the three-dimensional studies.

The three-dimensional analysis extends the results obtained in the two-dimensional study. It is seen that, despite the similarity of distribution (Fig. 20) and despite the close agreement of the 2-D stress-concentration factors with the average 3-D stress-concentration factor, the three-dimensional study is needed to identify the doubling of the stress-concentration factor in the middle of the dovetail slot. And, in addition, the three-dimensional work indicates the three-dimensional variation of stress with the addition of bending loads to the centrifugal load.

Table 1 — Comparison of 2-D and 3-D Stress-Concentration Factors

| Geometry and Load | Three-Dimensional Stress-Concentration Factors | | | Two-Dimensional Stress-Concentration Factors |
|---|--|------------|-----------------|--|
| | Maximum | Average | Overall Average | |
| Disk lug Centrifugal load Left tooth Right tooth | 9.6 7.9 | 5.2 5.0 | 5.1 | 5.2 |
| Centrifugal load and 12% circumferential load Left tooth Right tooth | 5.7 12.6 | 3.6 8.3 | 5.9 | — |
| Centrifugal load and 18% antiplane load Left tooth Right tooth | 10.6 10.5 | 5.8 5.3 | 5.5 | — |
| Blade Centrifugal load Convex side tooth Concave side tooth | 8.6 7.2 | 5.1 5.0 | 5.0 | 4.8 |

DISCUSSION OF RESULTS

Centrifugal Load

The dropoff of the stress at both ends of the teeth of the disk lug and blade (Figs. 10 and 11) can be taken as evidence that the bearing loads on the teeth drop off in much the same manner. And this in turn has to be attributed to the flexibility of the disk and/or blade at both ends. The disk is much more flexible at the ends than in the central region, and this probably accounts for most of the dropoff of stress and bearing loads at both ends. The blade becomes slightly more flexible at the leading and trailing edges of the airfoil, due to the taper, and may also contribute some to the dropoff.

Circumferential Load

As shown in Fig. 12, the clockwise circumferential load combined with the centrifugal load increases the stress in the right tooth of the disk lug and decreases it in the left, as might be expected. Also, since the fore end of the blade that contacts the right tooth of the disk lug is the furthest point from the axis of the moment, the maximum stress is shifted toward the fore end of the right tooth.

The maximum stress is not shifted to the *end* of the tooth, but is about one-third of the tooth length from the end. Even when the centrifugal component is taken out (Fig. 14), the maximum stress still seems to be about one-sixth of the length of the tooth from the end. The fact that the maximum stress does not occur at the end of the tooth seems to further emphasize the idea of flexibility at the fore and aft ends that was noted in the centrifugal loading.

This point is significant, since the fore end of the right tooth is where most of the failures have occurred, and the combination of centrifugal load with circumferential load might make a significant contribution to the failure load. The circumferential load could be vibrational or steady, due to gas load or circumferential acceleration of the engine.

Since the aft end of the left tooth is at the other extreme with respect to the fore end of the right tooth, and with respect to the axis of the moment, it might be expected that a negative peak similar to the positive peak on the right tooth might occur near the aft end. The negative peak on the left tooth (Fig. 14) occurs about the center. This suggests the possibility of liftoff of the tooth at the aft end due to the 12% circumferential load. Liftoff would violate the superposition principle applied to obtain the results in Figs. 14 and 15. If lift off did occur, these curves would probably be altered somewhat.

Antiplane Load

The analysis of antiplane load, Figs. 13, 15, 17, and 18, shows that a load acting from fore to aft end of the engine will produce similar stress distribution on both teeth of the disk lug, with the maximum shifted toward the fore end. When the centrifugal load is subtracted out (Fig. 15), the right tooth does actually show a maximum at the fore end of the tooth. However, when an axial load of 20% of the centrifugal is combined with the centrifugal load (Fig. 17), the maximum is still about one-third of the length of the tooth from the

fore end. The "skew" symmetry of both curves in Fig. 15 suggests that no liftoff occurred with 18% antiplane loading.

Out-of-Plane Load

The combination of the in-plane and antiplane analysis shows no significant stress buildup in directions other than the ones analyzed.

Superposition of Loads

In addition to the superposition results reported here (Figs. 16–19), a number of other curves could be constructed using the results in Figs. 10, 12, and 13. Thus the stress distributions in the *left* disk lug tooth for various combinations could be obtained just as they were for the right tooth in Figs. 16–19. Different three-component load combinations of centrifugal and either negative or positive values of antiplane and circumferential loads for both teeth could be developed, all from Figs. 10, 12, and 13. In all cases the superposition would require that the resulting load would not produce liftoff. This requirement could be roughly judged by using the appearance of negative stresses as an indication of liftoff.

SCALING

In general, there are several minor restrictions in applying photoelastic data to the actual structure. First, the loading of the photoelastic model cannot be such as to produce gross geometric distortions, unless such distortions also occur in the structure. This occasionally happens in thin-shelled structures, but is not a factor here. Second, the stresses in both the structure and the model must be within the linear stress-strain range of the materials. This is a necessary requirement that insures that, in both structure and model, stresses at every point are proportional to the applied load (e.g., reducing the load by half reduces all stresses by half). Third, for the analysis to be rigorous, the photoelastic material should have the same Poisson's ratio (ν) as the material of the structure. The titanium from which the disk and blades are made has a $\nu = 0.31$. The epoxy of the model, at the critical temperature at which the deformation and photoelastic response are produced, has a $\nu = 0.50$. Despite this marked difference, the influence on the surface stress distribution is considered small and can be neglected compared to other effects in this analysis.

The three restrictions taken together are not thought to influence the results more than the usual measurement errors. There is a restriction that is not generally applicable in photoelastic analysis, but in this particular case it must be considered. Because there is contact loading on the bearing surfaces, which may influence the distribution of load, and because the stress analysis is in the neighborhood of the bearing surfaces, to be rigorous in the stress analysis, the strains in both the structure and the model should be the same.

To satisfy this particular requirement the following equation must be satisfied:

$$\frac{P_m}{P_p} \frac{E_p}{E_m} \frac{\rho_p^2}{\rho_m^2} = 1,$$

where the subscripts m and p refer to model and prototype, and

$\frac{P_m}{P_p}$ is the load ratio

$\frac{E_p}{E_m}$ is the modulus ratio

$\frac{\rho_p}{\rho_m}$ is the geometric scaling factor.

Since model and prototype are in one-to-one geometric scale, the equation reduces to

$$P_m = \frac{E_m}{E_p} P_p$$

Young's modulus of titanium is 16.0×10^6 psi and of epoxy 2100 psi at the critical temperature. This gives

$$P_m = (1.31 \times 10^{-4}) P_p$$

At 10,500 rpm, a 0.738-lb blade acting at a radius of 10.75 in. will produce a centrifugal load of $P = 24,900$ lb. Ideally, the load per blade model in the photoelastic must be about 3 lb. To obtain sufficient response required actual model loads 2 to 5 times this amount. It was felt that the increased accuracy outweighed possible variations in contact loads.

CORRELATION OF STRESS WITH FAILURE ANALYSIS

A disk removed from service with a number of cracked lugs was analyzed in a parallel study [4] to this one. A number of lugs, cracked in service, were completely broken off in order to photograph and analyze the fracture surfaces. Two of the surfaces are shown in Fig. 2. It was found that the fatigue cracks in ten of the lugs extended from one-sixth to one-third the length of the right tooth from the fore end. It was difficult to identify the origin of the cracks in these teeth; however, it appears that many had multiple origins near the fore end of the right tooth. One crack never reached the fore end of the tooth. To relate these findings to the stress analysis requires consideration of the fractures and other factors such as fretting in the bearing area, as reported in Ref. 4.

SUMMARY

Three-dimensional photoelastic analysis of the disk/blade dovetail region of the TF-30 turbine engine third-stage fan indicates peak stresses in the disk and blade fillets that are an order of magnitude greater than the average stress in the neck of the disk lug. For centrifugal loading the peak stresses were found to occur in the central portion of the fillets with

PARKS AND SANFORD

pronounced dropoffs fore and aft. The dropoff was associated with the flexibility of the dovetail joint at both ends. The stresses at the center were twice those obtained in an earlier 2-D study.

Maximum stress concentrations found in the fillets of the disk lugs for representative loads are: 9.6 for centrifugal load; 12.6 for centrifugal load with 12% circumferential component; and 10.6 for centrifugal load with an 18% antiplane component.

REFERENCES

1. V. J. Parks and R. J. Sanford, "Experimental Stress Analysis of the TF-30 Turbine Engine Third-Stage Fan-Blade/Disk Dovetail Region," NRL Report 8149, Aug. 1977.
2. L. A. Beaubien, "Numerical Parametric Stress Analysis of the TF-30 Turbine Engine Third-Stage Fan-Blade/Disk Dovetail Region," NRL Memo Report 3671, Jan. 1978.
3. R. J. Sanford and J. W. Dally, "Stress Intensity Factors in the Third-Stage Fan Disk of the TF-30 Turbine Engine," NRL Report 8202, May 1978.
4. W. H. Vaughan, R. J. Sanford, J. M. Krafft, W. H. Cullen, and J. W. Dally, "Failure Studies of a Turbine Stage Fan Disk From a TF-30 Turbine Engine," NRL Memo Report 3874, Oct. 1978.
5. J. Cernosek, "Can Photoelasticity Be Cost-Effective in an Industrial Environment," *Proceedings of the SESA Spring Meeting* (extended summaries), Dallas, Texas, 15 May 1977. (Additional information in Bell Helicopter Textron letter of Sept. 27, 1977.)
6. R. J. Sanford and L. A. Beaubien, "Stress Analysis of a Complex Part: Photoelasticity vs Finite Elements," *Exper. Mech.* 17 (No. 12), 441-448 (Dec. 1977).